

# A relativistic partially electromagnetic planar plasma shock

M. E. Dieckmann<sup>1,2</sup>, P. K. Shukla<sup>1</sup> and L. O. C. Drury<sup>2</sup>

<sup>1</sup>*Institute of Theoretical Physics IV and Centre for Plasma Science and Astrophysics,  
Ruhr-University Bochum, D-44780 Bochum, Germany*

<sup>2</sup>*Dublin Institute for Advanced Studies, 5 Merrion Square, Dublin 2, Ireland*

(Dated: October 9, 2018)

We model relativistically colliding plasma by PIC simulations in one and two spatial dimensions, taking an ion-to-electron mass ratio of 400. Energy dissipation by a wave precursor of mixed polarity and different densities of the colliding plasma slabs results in a relativistic forward shock forming on millisecond timescales. The forward shock accelerates electrons to ultrarelativistic energies and reflects upstream ions, which drag the electrons along to preserve the plasma quasi-neutrality. No reverse shock forms. The shock may be representative for internal gamma ray burst shocks.

PACS numbers: 98.70.Rz, 52.35.Tc, 52.65.Rr, 52.27.Ny

Accreting compact objects like neutron stars or black holes are amongst the most energetic environments in the universe. Such systems can range from microquasars through active galactic nuclei to gamma ray bursts (GRBs) [1, 2, 3, 4]. Common to these objects is the ejection of a relativistic jet that is probably accelerated by magnetic fields [5, 6]. GRB jets are ejected by a forming compact object [7]. Their high Lorentz factor  $100 < \Gamma < 10^3$  introduces a radiation beaming, making GRBs detectable at cosmological distances. The GRB emissions are explained either by the fireball model, in which the plasma kinetic energy dominates [1, 2], or by the electromagnetic model, in which the Poynting flux is dominant [8, 9]. We consider the fireball model.

The high energies involved in the thermalisation of relativistic jets imply that plasma structures form, such as phase space holes [10]. A shock description needs a kinetic approach [11]. Particle-in-cell (PIC) simulations have modelled the external GRB shock between the jet and the ambient plasma [12, 13, 14, 15, 16, 17], and have examined the magnetic field amplification and particle acceleration. The weakly magnetized external GRB shocks develop out of a broad wave spectrum [18, 19, 20, 21], and are thus filamentary. The internal shocks, powering the prompt emissions, form closer to the collapsing star with its strong magnetic fields. The magnetic field pressure may initially exceed the thermal pressure of the jet plasma, in contrast to the case considered by Ref. [18]. The magnetic field and the high plasma temperature [22] suppress the filamentation modes [23, 24, 25] and other wave modes can develop.

The finite grid instability requires a high spatial resolution on electron timescales of multi-dimensional PIC simulations [26], while a relativistic shock will extend over ion scales. A large ion-to-electron mass ratio is required to model shocks [27]. To account for these constraints, we select the initial conditions such as to physically confine the plasma dynamics to one spatial dimension (1D) and three momentum components, which allows us to restrain also the simulation geometry to one spatial dimension. We verify the validity of this assumption with the help of a two-dimensional (2D) simulation. We demon-

strate that the magnetic field results in the formation of a relativistic planar shock. The energy dissipation is provided by a wave with mixed electrostatic and electromagnetic polarity, probably a nonlinear oblique whistler [28]. This contrasts the energy dissipation by the purely electromagnetic filamentation modes considered in Refs. [13, 14, 15, 16, 17, 24], and the nonrelativistic electrostatic shocks modelled in Refs. [27, 29]. Different slab densities [29] facilitate the development of a shock with a Mach number of 40 and an Alfvénic Mach number of 10. The forward shock reflects upstream ions.

PIC simulation methods [30] solve the Maxwell equations and the relativistic equation of motion

$$\nabla \times \mathbf{E} = -\frac{\partial \mathbf{B}}{\partial t}, \quad (1)$$

$$\nabla \times \mathbf{B} = \mu_0 \mathbf{j} + \mu_0 \epsilon_0 \frac{\partial \mathbf{E}}{\partial t}, \quad (2)$$

$$\frac{d\mathbf{p}_i}{dt} = \frac{q_j}{m_j} (\mathbf{E} + \mathbf{v}_i \times \mathbf{B}), \quad (3)$$

and fulfill  $\nabla \cdot \mathbf{B} = 0$  and  $\nabla \cdot \mathbf{E} = \rho/\epsilon_0$  as constraints. The electric  $\mathbf{E}$  and magnetic  $\mathbf{B}$  fields are defined on a discrete grid. Each computational particle (CP) with index  $i$  of the species  $j$  has the charge  $q_j$  and mass  $m_j$  with  $q_j/m_j = q/m$ , where  $q$  and  $m$  are the physical charge and mass of the particles, represented by the species  $j$ . The particle momentum is  $\mathbf{p}_i = m_i \mathbf{v}_i \Gamma(\mathbf{v}_i)$ .

Two plasma slabs collide in the simulations at the position  $x = 0$ , each consisting of the electrons and ions. The ion-to-electron mass ratio is  $R = m_i/m_e = 400$ . The plasma frequency of the species  $j$  with the number density  $n_j$  is  $\omega_{p,j} = (n_j q_j^2 / m_j \epsilon_0)^{1/2}$ . The electrons of slab 1 have  $\omega_{p,1} = 10^5 \times 2\pi/s$  and the ions  $\omega_{p,2} = \omega_{p,1}/\sqrt{R}$ . The dense slab 1 is initially moving with the positive speed  $v_b$  along the  $x$ -direction. The electrons and ions of slab 2 have  $\omega_{p,3} = \omega_{p,1}/\sqrt{10}$  and  $\omega_{p,4} = \omega_{p,3}/\sqrt{R}$ , respectively. The tenuous slab 2 moves with the speed  $-v_b$  along the  $x$ -direction. Initially, all mean speeds along the  $y, z$  directions vanish. All plasma species have the observed jet temperature  $T = 100$  keV [22]. The position and time have the units of the electron skin depth

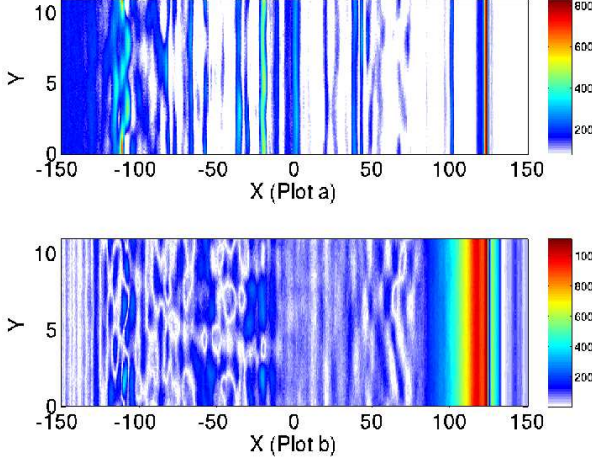


FIG. 1: (Color online) The electric fields in V/m in the 2D simulation at  $t = t_2$ : (a) shows the flow-aligned electric field component  $E_x$  and (b) shows  $E_y$ , the second electric field component in the simulation plane.

$\lambda_s = c/(\omega_{p,1}^2 + \omega_{p,3}^2)^{1/2}$  and  $\lambda_s/c$ , where  $c$  is the speed of light in vacuum. Each slab initially occupies half of the simulation box. The slabs collide along the  $x$ -direction at the speed  $v_c = 2v_b/(1 + v_b^2) = 0.9c$ , which is representative of internal GRB shocks [2]. We introduce a spatially homogeneous oblique magnetic field. The magnetic field component with  $eB_x/m_e = \sqrt{2}\omega_{p,1}$  suppresses the filamentation instability [23] and a perpendicular  $B_z = B_x/10$  enhances the energy dissipation. Initially, we set  $B_y = 0$ . The initial magnetic field strength is thus  $5\mu T$ . The initial box-averaged plasma kinetic energy density exceeds the magnetic field energy density by a factor of  $10^4$ . The 1D simulation box length is  $L = 1.58 \times 10^4 \lambda_s$ , which is resolved by  $1.8 \times 10^5$  cells. The 2D box has the extent  $L_x = 714 \lambda_s$  ( $1.6 \times 10^4$  cells) and  $L_y = 11 \lambda_s$  (200 cells) along the  $x$  and  $y$  directions, respectively. The boundary conditions are periodic. The 1D (2D) simulation time is  $t_1 = 4370$  ( $t_2 = 194$ ). The 2D simulation represents each plasma species by 64 particles per cell (PPC). The 1D simulation resolves each species of the dense (tenuous) slab by 576 (256) PPC.

The electric field in the 2D simulation plane at  $t = t_2$  in Fig. 1 reveals a planar structure at  $x \approx 120$ , the leading edge of the dense plasma slab. A similar  $E_z$  distribution is not shown. The filamentation instability would lead to the structure formation on a scale of  $\lambda_s$  along  $y$ , and it is here suppressed by  $B_x$  [23]. No strong field is present at  $x \approx -120$ . We exploit the planarity of the slab front in Fig. 1 and resort to the 1D simulation with its better statistical plasma representation.

The current system responsible for the electric fields in Fig. 1 is displayed in Fig. 2. The electrons of the tenuous slab are deflected by the oblique magnetic field that is frozen into the dense downstream plasma. Since the massive upstream ions are not significantly deflected,

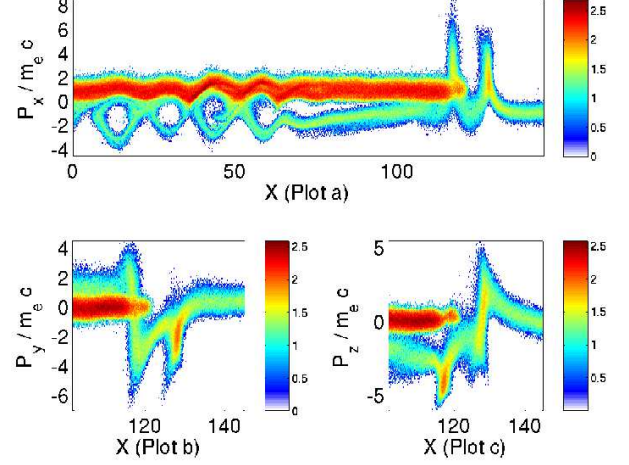


FIG. 2: (Color online) The 10-logarithms of the electron distributions in the 1D simulation at  $t = t_2$ : The distribution in the  $x, p_x$  plane is shown in panel (a). Panels (b) and (c) display the distributions in the  $x, p_y$  and  $x, p_z$  planes.

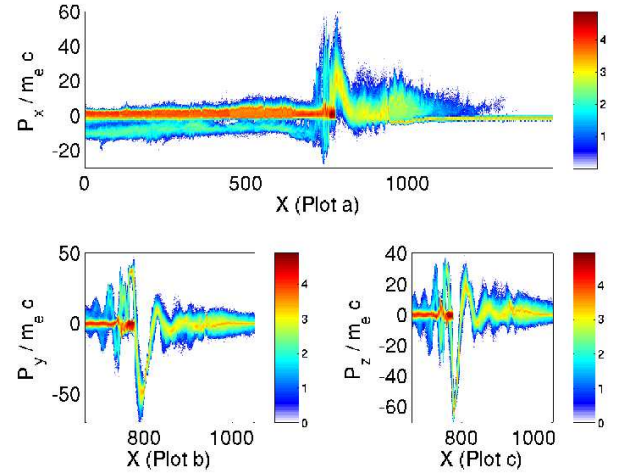


FIG. 3: (Color online) The 10-logarithms of the electron distributions in the 1D simulation at  $t = 1550$ : Panel (a) shows the distribution  $x, p_x$ . The distributions in  $x, p_y$  and  $x, p_z$  are exhibited in panels (b) and (c), respectively.

a current and thus the electric field is building up at the leading edge of the plasma slab in Fig. 1. Further downstream, Fig. 2(a) shows the electron phase space holes, which thermalize the electrons, as in Ref. [25]. These are also observed at the Earth bow shock [31].

The energy dissipation by the electric fields eventually modulates the electrons of the dense plasma slab, giving rise to larger electric fields. Consequently, Fig. 3 demonstrates that the electrons are accelerated to  $\Gamma$  factors of tens to hundreds and follow a corkscrew orbit. The relativistic mass of the electrons is not small compared to  $m_i = 400 m_e$  at  $t = 1550$ . Figure 4(a) shows the ion re-

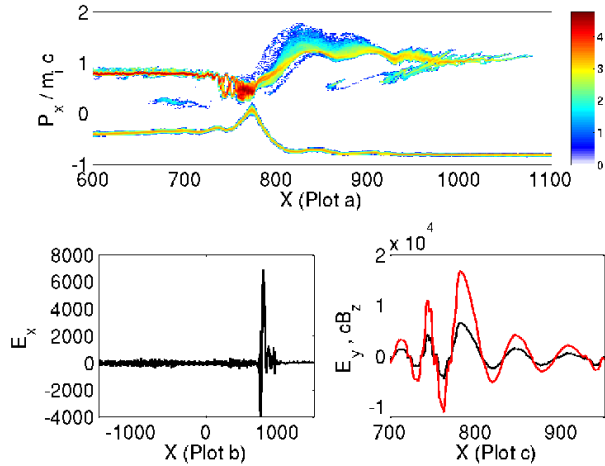


FIG. 4: (Color online) Panel (a) shows the ion distribution in  $x, p_x$  space. The color is the 10-logarithm of the number of CPs. Panel (b) shows the electrostatic  $E_x$  field and panel (c) shows  $E_y$  and  $cB_z$  (red). The time is  $t = 1550$ .

sponse to the strong fields. The spatial interval with the strongest particle acceleration at  $x \approx 780$  is well behind the expected slab front  $v_b t/\lambda_s \approx 980$  at  $t = 1550$ . Some ions have been accelerated beyond the initial velocity  $v_b$  by the electric field at the slab front [25] and they have propagated farther upstream beyond  $x \approx 980$ .

The wave modes at  $x \approx 800$  that grow only close to the leading edge of the dense plasma slab, as Fig. 4(b) exemplifies for the  $E_x$  field component, could have originated from an oblique whistler instability, similar to that discussed in Ref. [28]. The wave growth at  $x < 0$  is suppressed or delayed. This will introduce an asymmetric plasma dynamics in the intervals separated by  $x = 0$ .

The wave amplitudes in the considered plasma scale linearly with  $\omega_{p,1}$  if all ratios between  $\omega_{p,j}$  remain the same as discussed, for example, in Ref. [32]. The wave is circularly polarized, which explains the electron corkscrew orbits in Fig. 3. The peak value of  $B_z$  in Fig. 4(c) exceeds the initial background magnetic field  $B_0 = (B_x^2 + B_z^2)^{1/2}$  with  $cB_0 \approx 1500$  V/m, and the wave in Fig. 4(c) is nonlinear. The mixed polarity of the waves allows them to interact with the plasma through their electrostatic component. The wave amplitude is sustained, because the wave is driven by the dense plasma slab that compensates damping losses. The damping may explain why  $E_y$  and  $B_z$  are in phase in Fig. 4(c).

At  $t = t_1$ , the ion distribution in Fig. 5(a) has developed into a shock. The foreshock in the interval  $2000 < x < 3200$  is formed by incoming and shock-reflected ions. The electron transport with the shock-reflected ions across the upstream  $\mathbf{B}$  in Fig. 5(b) ensures the plasma quasi-neutrality. The two ion beams at  $x < 500$  result from the delayed shock formation. At  $x \approx 1800$ , the  $p_x$  values of the electrons are comparable to those of the ions multiplied by  $m_i/m_e$  in the simu-

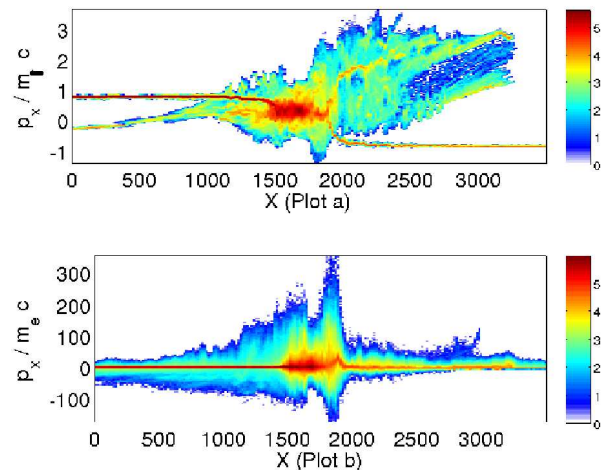


FIG. 5: The shock: (a) shows the ion distribution in  $x, p_x$ , while (b) shows the corresponding electron distribution. The color is the 10-logarithm of the number of CPs.

lation reference frame. A Lorentz transformation of the electron velocity into the upstream frame, which moves with  $v = -v_b$  relative to the simulation box frame, yields a peak electron  $\Gamma \approx 700$  for our  $v_c = 0.9c$ . In comparison, the filamentation instability in Ref. [17] yields only a peak electron  $\Gamma \approx 10$  for a collision speed  $v_f$  with  $\Gamma(v_f) = 5$ . The planar electromagnetic shock considered here is a stronger electron accelerator.

The shock in Fig. 5 has formed during the time  $t = t_1$ , which is 7 ms in physical units. If we assume that this shock would constitute an internal shock of a GRB and that the jet frame moves at a  $\Gamma \approx 10^3$ , the time dilation would yield a duration of seconds for the shock development in the Earth (observer) frame of reference. This is comparable to the timescale of the prompt emissions. The shock we consider is likely to form during a longer time for  $m_i/m_e = 1836$ . The bulk Lorentz factor of GRB jets may, however, also be less than  $10^3$  [3]. Different jet plasma densities, which may be higher than we consider in this work [33], do not strongly affect the shock development time due to a scaling of the timescales with the square root of the density [32].

In summary, we have examined the collision of two plasma slabs with different densities at a relativistic speed. The bandwidth required to model the plasma dynamics at a high ion-to-electron mass ratio cannot be realized at present with PIC simulations in more than one spatial dimension due to the necessary large box size [3] and the high-resolution grids that are required in higher dimensions to suppress the electromagnetic finite grid instability [26]. The quasi-parallel magnetic field has, however, suppressed the beam filamentation, and the initial planar shock development may thus be well-approximated by a one-dimensional PIC simulation. The energy dissipation has been accomplished through a nonlinear wave of mixed polarity, which could have origi-

nated from an oblique whistler instability. Whistlers are frequently observed also at slower quasi-parallel plasma shocks and they are known to be efficient particle accelerators [34]. The large energy dissipation, which ultimately forces the shock to form, is likely to distort the guide magnetic field and the slab boundary would likely be deformed by the ram pressure exerted by the upstream plasma. However, a significant distortion of the guide magnetic field away from the flow-aligned direction introduces a stronger perpendicular magnetic field component. The latter will probably not suppress or delay the shock formation and the plasma thermalization. Our simulation may thus give a correct estimate for the shock formation time even in 3D.

The shock we consider here may thus be representative for a GRB internal shock. Such a rapid shock formation

has previously been questioned, at least for purely electromagnetic or electrostatic shocks [35]. A Lorentz boost of the electron energy by a transformation from the jet frame into the Earth frame results in electron energies in the GeV-TeV range and could be further enhanced by the thermalization of the shock-reflected ion beam [32, 36]. The shock-accelerated electrons undergo rapid velocity changes at the shock, and may radiate through synchrotron emission [37] and bremsstrahlung [38]. The suppressed or delayed development of a reverse shock in our simulation may explain the absence of reverse shock signatures in GRB prompt emissions [9].

**Acknowledgments:** The DFG (grant SH-21/1-1) and the DIAS (Ireland) have funded this work. The Irish ICHEC and the Swedish HPC2N computer centres have provided computational facilities and support.

- 
- [1] T. Piran, *Rev. Mod. Phys.* **76**, 1143 (2004).
  - [2] T. Piran, *Phys. Rep.* **314**, 575 (1999).
  - [3] E. Waxman, *Plasma Phys. Controll. Fusion* **48**, B137 (2006).
  - [4] J. A. Zensus, *Ann. Rev. Astron. Astrophys.* **35**, 607 (1997); R. Fender and T. Belloni, *Ann. Rev. Astron. Astrophys.* **42**, 317 (2004).
  - [5] R. D. Blandford and D. G. Payne, *Mon. Not. R. Astron. Soc.* **199**, 883 (1982); R. D. Blandford and R. L. Znajek, *ibid.* **179**, 433 (1977).
  - [6] K. I. Nishikawa *et al.*, *Astrophys. J.* **625**, 60 (2005).
  - [7] S. Campana *et al.*, *Nature* **442**, 1008 (2006).
  - [8] C. Thompson, *Mon. Not. R. Astron. Soc.* **270**, 480 (1994); M. Lyutikov and R. Blandford, *astro-ph/0312347* (2003).
  - [9] M. Lyutikov, *New J. Phys.* **8**, 119 (2006).
  - [10] K. V. Roberts and H. L. Berk, *Phys. Rev. Lett.* **19**, 297 (1967); H. Schamel, *Phys. Plasmas* **7**, 4831 (2000); B. Eliasson and P. K. Shukla, *Phys. Rep.* **422**, 225 (2006).
  - [11] H.-J. Fahr and M. Siewert, *Astron. Astrophys.* **458**, 13 (2006).
  - [12] K. I. Nishikawa *et al.*, *Astrophys. J.* **595**, 555 (2003).
  - [13] L. O. Silva *et al.*, *Astrophys. J.* **596**, L121 (2003).
  - [14] R. A. Fonseca *et al.*, *Phys. Plasmas* **10**, 1979 (2003).
  - [15] C. B. Hededal *et al.*, *Astrophys. J.* **617**, L107 (2004).
  - [16] J. T. Frederiksen *et al.*, *Astrophys. J.* **608**, L13 (2004).
  - [17] K. I. Nishikawa *et al.*, *Astrophys. J.* **642**, 1267 (2006).
  - [18] M. V. Medvedev and A. Loeb, *Astrophys. J.* **526**, 697 (1999).
  - [19] A. Bret, M.-C. Firpo and C. Deutsch, *Phys. Rev. Lett.* **94**, 115002 (2005).
  - [20] A. Bret, *Europhys. Lett.* **74**, 1027 (2006).
  - [21] R. C. Tautz, I. Lerche and R. Schlickeiser, *Phys. Plasmas* **13**, 052112 (2006); U. Schaefer-Rolfs, I. Lerche and R. Schlickeiser, *ibid* **13**, 012107 (2006).
  - [22] F. Ryde, *Astrophys. J.* **614**, 827 (2004).
  - [23] A. Bret, M. E. Dieckmann and C. Deutsch, *Phys. Plasmas* **13**, 082109 (2006).
  - [24] C. B. Hededal and K. I. Nishikawa, *Astrophys. J.* **623**, L89 (2005).
  - [25] M. E. Dieckmann, P. K. Shukla and B. Eliasson, *New J. Phys.* **8**, 255 (2006).
  - [26] M. E. Dieckmann *et al.*, *Phys. Plasmas* **13**, 112110 (2006).
  - [27] M. Scholer and S. Matsukiyo, *Ann. Geophys.* **22**, 2345 (2004).
  - [28] J. Zhao, J. I. Sakai and K. I. Nishikawa, *Solar Phys.* **168**, 345 (1996); R. Ciurea-Borcia *et al.*, *Phys. Plasmas* **7**, 359 (2000).
  - [29] G. Sorasio *et al.*, *Phys. Rev. Lett.* **96**, 045005 (2006).
  - [30] J. W. Eastwood, *Comput. Phys. Commun.* **64**, 252 (1991).
  - [31] S. D. Bale *et al.*, *Astrophys. J.* **575**, L25 (2002).
  - [32] M. E. Dieckmann, P. K. Shukla and B. Eliasson, *Phys. Plasmas* **13**, 062905 (2006).
  - [33] A. Panaitescu and P. Meszaros, *Astrophys. J.* **492**, 683 (1998).
  - [34] Y. Kuramitsu and V. Krasnoselskikh, *Phys. Rev. Lett.* **94**, 031102 (2005); A. Levinson, *Astrophys. J.* **401**, 73 (1992).
  - [35] J. J. Brainerd, *Astrophys. J.* **538**, 628 (2000).
  - [36] K. G. McClements *et al.*, *Mon. Not. R. Astron. Soc.* **291**, 241 (1997).
  - [37] S. M. Tang and S. N. Zhang, *Astron. Astrophys.* **456**, 141 (2006).
  - [38] R. Schlickeiser, *Astron. Astrophys.* **410**, 397 (2003).